ACS APPLIED MATERIALS & INTERFACES

Research Article

www.acsami.org

In Situ Integration of Squaraine-Nanowire-Array-Based Schottky-Type Photodetectors with Enhanced Switching Performance

Yuping Zhang,[†,§] Wei Deng,[†,§] Xiujuan Zhang,*[,†] Xiwei Zhang,[†] Xiaohong Zhang,*[,‡] Yuliang Xing,[†] and Jiansheng Jie*[,†]

[†]Institute of Functional Nano & Soft Materials (FUNSOM), Jiangsu Key Laboratory for Carbon-Based Functional Materials & Devices, Soochow University, Suzhou, Jiangsu 215123, P. R. China

[‡]Nano-organic Photoelectronic Laboratory and Key Laboratory of Photochemical Conversion and Optoelectronic Materials, Technical Institute of Physics and Chemistry, Chinese Academy of Science (CAS), Beijing 100190, P. R. China

Supporting Information

ABSTRACT: Organic nanostructure-based photodetectors are important building blocks for future high-performance, low-cost, flexible nano-optoelectronic devices. However, device integration remains a large challenge, and the structure-dependent performance of the device has been seldom studied. Here, we report the in situ integration of 2,4-bis[4-(*N*,*N*-dimethylamino)phenyl]squaraine (SQ)-nanowire (NW)-array-based photodetectors by growing the organic NW arrays on prefabricated electrodes through an evaporation-induced self-assembly process. In contrast with ohmic-contact devices, asymmetric electrode pairs of Au−Ti were utilized to achieve the construction of Schottky-type photodetectors on the basis of organic NW arrays. Significantly, the Schottky-type photodetectors exhibited a significantly enhanced performance as compared to the ohmic-type devices in terms of their higher photosensitivity and switching speed. The presence of a strong built-in electric field at the junction interface, which greatly facilitated the separation/transportation of photogenerated electron−hole pairs, was suggested to be responsible for the superior performance of the Schottky-type photodetectors. More importantly, the organic NW-array-based devices also showed a higher sensitivity and reproducibility than that of the single NW-based devices, and they were capable of low-light detection. The investigation of the photodetector circuitry also disclosed a very low pixel-to-pixel variation owing to the average effect of the NW-array-based devices. It is expected that organic NW-array-based Schottky-type photodetectors will have important applications in future organic nano-optoelectronic devices.

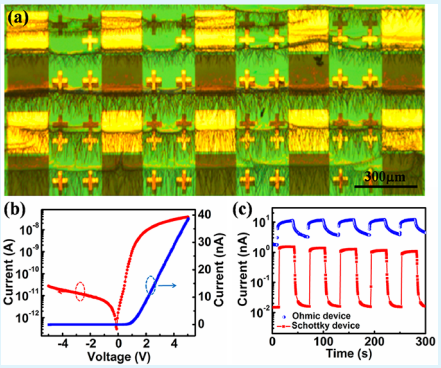

KEYWORDS: *SQ nanowires, organic nanowire arrays, self-assembly, Schottky diodes, photodetectors*

INTRODUCTION

Among various distinct types of nanostructures, small-molecule organic semiconductor nanostructures constitute a unique category with regard to their outstanding characteristics such as tailored electronic and optical properties via molecular design as well as their potential for use in flexible and stretched electronics.[1] Some unique applications have been successfully achieved for organic nanostructures, such as solar cells,[2,3] optical waveguides and lasers,[4−6] field-effect transistors,[7−11] and photodetectors,[12−16] which demonstrates their great potential as building blocks for the next generation of miniaturized electronic and optoelectronic devices. Notably, small-molecule organic nanostructure-based photodetectors have drawn particular attention because of their much broader response spectrum compared to their inorganic counterparts as well as their significantly higher sensitivity than that of their bulk and film materials,[15,17,18] which would find potential applications in imaging, optical communication, future memory storage, and optoelectronic circuits.[19,20] The most typical configuration for organic nanostructure-based photodetectors uses single or multiple nanowires (NWs)/nanotubes as the essential building block, which forms good ohmic contacts with electrodes to minimize the contact resistance and highlight the effect from the changes in the resistance/surface states of the nanostructures.[21] However, the performance randomness and instability of the individual nanostructure-based devices have become critical issues, obstructing their wide applications and the further exploitation of their technical promise. The large-scale assembly of NW arrays with controlled orientations and interspacing provides an effective way to achieve devices with improved performance and enhanced stability to satisfy their practical applications.[22,23] However, unlike the vapor−liquid−solid (VLS) growth of inorganic NW arrays in which the NW dimension, position, and orientation could be well controlled by the metallic catalysts,[24] organic NWs are normally fabricated via a self-assembly method, and their controllable synthesis is

Received: May 31, 2013
Accepted: July 26, 2013
Published: July 26, 2013

more difficult.[25] Also, conventional device-processing techniques, such as photolithography, are not suitable for the organic nanostructures because of the inferior chemical/physical stability of organic materials. Therefore, it remains a great challenge to achieve integrated devices based on organic nanostructures.

However, organic nanostructure-based photodetectors in current reports always choose an ohmic-type device structure,[17,26] (i.e., a device with ohmic contacts at both ends in which the optical signal is reflected by the resistance variation of the organic nanostructures under light illumination). This device architecture can ensure the maximum presence of the intrinsic feature of the nanostructures but with no other contributions for the device performance improvement. Recently, the Schottky-type device structure has been widely employed in sensors,[27,28] light-controlled diodes,[29] and solar cells,[30,31] where the presence of a Schottky junction at the semiconductor/electrode interface can effectively facilitate charge separation/transport and thus lead to a significant performance improvement. It is known that for an ideal photodetector fast response speed and high sensitivity are essential characteristics.[32] To date, Schottky-type photodetectors based on various inorganic nanostructures with enhanced sensitivity and switching speed have been successfully demonstrated.[28,33] It stands to reason that the employment of a Schottky-type device structure for organic nanostructure-based photodetectors may also provide a feasible way to realize the high performance of the devices. To achieve this aim, however, it is essential to overcome the difficulties in organic nanostructure assembly and device construction.

Herein, we report a one-step large-scale integration of 2,4-bis[4-(*N*,*N*-dimethylamino)phenyl]squaraine (SQ)-NW arrays for Schottky-type photodetector circuitry with largely enhanced sensitivity and fast switching speed. By implementing our recently developed evaporation-induced self-assembly method, large-scale SQ-NW arrays can be patterned to grow on prefabricated electrodes with controlled interspacing on the substrate and can be configured as integrated photodetectors, avoiding direct photolithography on the organic nanostructures. Owing to the presence of a Schottky junction, SQ-NW-array-based Schottky-type photodetectors exhibited a much higher sensitivity and faster switching speed than that of ohmic-type photodetectors. More interestingly, NW-arrays-based devices also demonstrated remarkably enhanced photoresponse properties compared to single NW-based photodetectors. We further measured the integrated photodetector circuits, and a very small pixel-to-pixel variation in the distribution of pixel photosensitivity was found. The high yield of the operational pixels with a high level of integration unambiguously demonstrates the potential of this assembly strategy for large-scale organic nanostructure-based electronic and optoelectronic device integration.

EXPERIMENTAL DETAILS

SQ-NW arrays were fabricated using an evaporation-induced self-assembly method. For the detailed fabrication process, refer to our previous work.[34] In a typical experiment, the clean substrate, such as a Si wafer, was immersed vertically into a SQ/dichloromethane (CH_2Cl_2) solution (5 mL, 0.04 mM) in a container at room temperature. The CH_2Cl_2 was then allowed to gradually evaporate. A higher evaporation rate at the liquid/substrate interface would increase the local concentration of molecules and lead to nucleation of NWs when a critical concentration is reached. The NWs can self-assemble into aligned arrays at the contact line and pattern on the substrate in parallel stripes. After the solvent evaporated completely, eyelash-like aligned SQ-NW arrays were grown over the entire substrate.

To construct the Schottky-type SQ-NW-array-based photodetectors, Ti (50 nm)−Au (50 nm) electrode pairs were fabricated on a SiO_2 (300 nm)/Si substrate via two-step UV photolithography and lift-off processes. Au and Ti in the electrode pairs served as the Schottky and ohmic contacts for the devices, respectively. SQ-NW arrays were grown on the electrode pairs according to the aforementioned approach. The dewetting rate was adjusted to 1.2 mm/min to maintain a NW array interval of ∼150 μm, which showed little variation from the top to the bottom of the substrate. By this means, aligned NW arrays could be properly deposited across the predefined electrode pairs, allowing the in-situ integration of the NW-array-based photodetectors.

The morphologies of the SQ-NW arrays were investigated using a fluorescence microscope (Laica DM4000M) with an attached digital camera (Olympus C-5060). For transmission electron microscopy (TEM) investigation, the NWs were first scraped from the growth substrate and dispersed in water. A drop of the dispersion was then drop casted onto a holey carbon film supported on a copper TEM sample grid. After drying in air, the TEM sample was observed with a Philips CM300FEG TEM operated at an accelerating voltage of 80 kV. Ultraviolet photoelectron spectroscopy (UPS) data was collected in a Kratos AXIS Ultra^{DLD} ultra-high-vacuum (UHV) surface analysis system. The X-ray source was generated from a monochromatic aluminum Kα source (1486.6 eV). He I (21.2 eV) radiation lines generated by a discharge lamp were used in the UPS measurements, and the signals were collected by a hemispherical analyzer.

Electrical measurements of the devices were conducted with a semiconductor characterization system (Keithley 4200). The temperature-controlled experiments were performed using a Lake Shore CRX-4K/CRTTP6 cryogenic probe station under vacuum conditions. The white light emitted by the optical microscope on the probe station was used as the white-light source, with a light intensity of ∼0.1 mW/cm^2. Monochromatic light (600 nm) was obtained by filtering the white light with an optical filter. The 600 nm light intensity was tuned between 2.9 and 30.7 μW/cm^2 to measure the light-intensity-dependent photocurrent.

RESULTS AND DISCUSSION

SQ-NWs were selected as the model compound to study the device structure-dependent photoconductive characteristics owing to their excellent optoelectronic properties.[35−40] To achieve the in situ integration of the SQ-NW-array-based photodetectors, the SiO_2/Si substrate with prefabricated electrode arrays was immersed vertically into a SQ/CH_2Cl_2 solution (Figure 1a). CH_2Cl_2 was then allowed to gradually evaporate, leading to the precipitation of the SQ-NW arrays at the liquid/substrate interface. It is known that both the ground and excited states of SQ are intramolecular donor−acceptor−donor charge-transfer (D−A−D CT) states.[41] This type of molecule can easily aggregate and grow into 1D nanostructures in a "slipped stack" arrangement directed by the strong intermolecular interactions between the acceptor (A) and the donor (D) groups under appropriate conditions (Supporting Information, Figure S1). The interval of the adjacent SQ-NW arrays can be adjusted by controlling the solution evaporation rate to fit with the interval of the electrode pairs. As a result, eyelash-like aligned SQ-NW arrays were directly grown across the prefabricated electrodes, forming a typical bottom-contact device, as shown in Figure 1b,c. There are approximately dozens of aligned NWs on each device with uniform morphologies. The TEM image in Figure 1d shows that the SQ NWs have a smooth surface.

Figure 1e schematically illustrates the device configuration. The adjacent Au−Au electrodes with the SQ-NW array

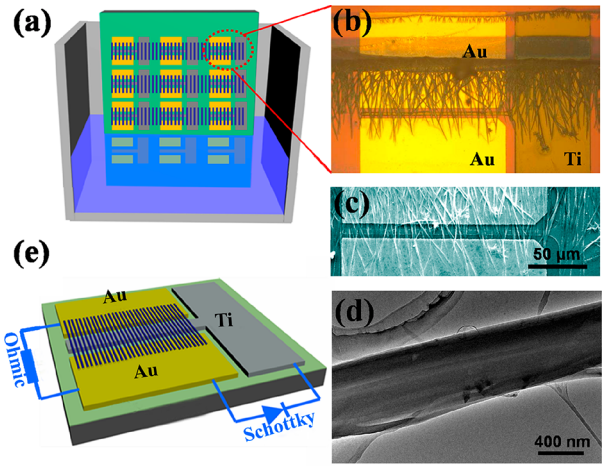

Figure 1. (a) Schematic illustration of the dip-coating set up for the in situ integration of SQ-NW-arrays-based photodetectors. (b) Optical microscope image of an individual Schottky-type device. Ti (50 nm) and Au (50 nm) serve as the Schottky and ohmic contacts in the device, respectively. (c) Enlarged SEM image of the device. (d) Representative TEM image of a single SQ NW. (e) Schematic illustration shows the device configuration for ohmic-type and Schottky-type devices.

construct an ohmic-type device, which was verified by the linear current versus voltage (I–V) curve (Figure 2a), whereas the

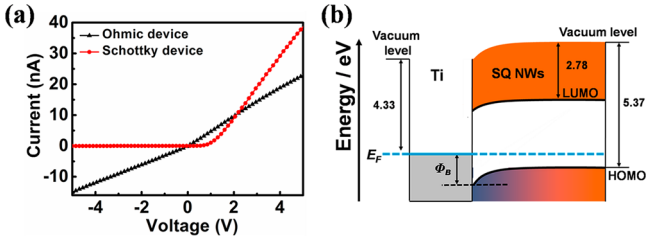

Figure 2. (a) I–V characteristics of the SQ-NW-arrays-based ohmic- and Schottky-type devices. (b) Schematic energy-band diagram of the Ti/SQ-NW-array Schottky junction. LUMO and HOMO represent the lowest unoccupied molecular orbital level and the highest occupied molecular orbital level of the SQ NW, respectively.

asymmetric metal electrodes (Au–Ti) with the SQ-NW array form a Schottky-type device in which obvious rectifying behavior is observed (Figure 2a). Measurements on several different NW arrays exhibited similar results, indicating the good reproducibility of the devices. As such, the device performance can be compared directly between ohmic-type and Schottky-type devices. The HOMO and LOMO levels of the SQ NWs were determined to be 5.37 and 2.78 eV, respectively, on the basis of the UPS measurements (Supporting Information, Figure S2). Therefore, the principle of the SQ-NW array/Ti Schottky-type device can be understood by plotting the energy-band diagram, as displayed in Figure 2b. SQ is a typical p-type semiconductor; hence, a high Schottky barrier will exist at the SQ-NW array/Ti interface because of the large difference of the SQ's HOMO level with the work function of Ti (4.33 eV). In contrast, Au with a large work function of 5.1 eV can form an ohmic contact with the SQ-NW array. As a result, the I–V curve measured between two adjacent Au electrodes shows good linearity, whereas the curve between Au and Ti exhibits rectifying behavior.

To gain more insight into the SQ-NW array/Ti Schottky diode, temperature (T)-varied measurements were conducted, as shown in Figure 3. From the logarithmic plot of the I–V

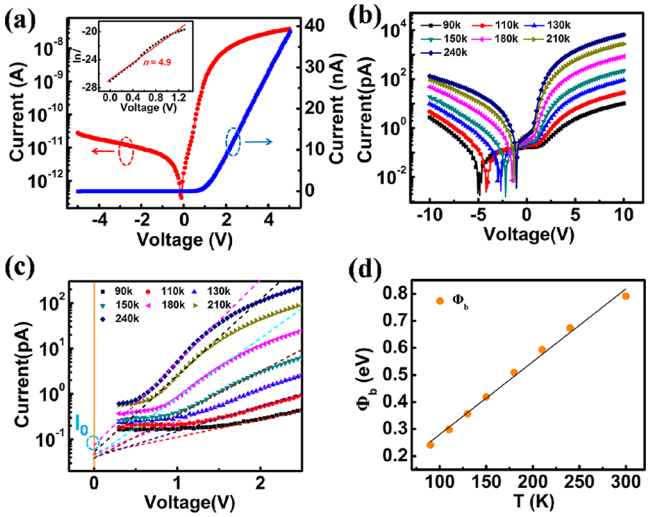

Figure 3. (a) Rectifying characteristics of the SQ-NW array/Ti Schottky diode measured in dark. The inset shows the natural logarithmic plot of the I–V curve (symbols), which is fitted by a straight line at the low-voltage region to deduce the ideality factor n. (b) Rectifying characteristics measured at varied temperature ranging from 90 to 300 K. (c) I_0 at varied temperature is deduced by extrapolating the I–V curves to the vertical axis at V = 0 V. (d) Dependence of barrier height Φ_b on temperature.

curve at room temperature in the dark (Figure 3a), it can be seen that the device exhibits excellent diode characteristics; the current on/off ratio is as high as ~10^3 at a voltage range of ±5 V, which is much higher than the typical value for organic film Schottky diodes.[42−45] Meanwhile, the turn-on voltage is deduced to be ~0.85 V. The high rectification ratio along with the small turn-on voltage indicates the high quality of the SQ-NW array/Ti Schottky junction formed via the in situ integration method. The I–V characteristics of the Schottky junction can be described by the following equation[46]

$$I = I_0\left[\exp\left(\frac{qV}{nkT}\right) - 1\right] \approx I_0 \exp\left(\frac{qV}{nkT}\right) \quad (1)$$

where I_0 is the reverse saturation current, n is the ideality factor, q is the electronic charge, k is the Bolzmann's constant, and T is the absolute temperature. On the basis of the above equation, the ideality factor n can be deduced to be ~4.9 by fitting the straight part of the semilog I–V curve at the low-voltage region (inset in Figure 3a). This value is larger than that for an ideal diode (n = 1), implying the existence of the impurities and defects at the organic NW array/Ti interface, which may be formed during the solution growth process. However, the enhanced tunneling current for the nanoscale junction could be another important reason for the large n value observed.[47] The I–V characteristics of the SQ-NW array/Ti Schottky diode were further investigated at varied temperatures of 90, 110, 130, 150, 180, and 210 K, respectively, in the dark, as shown in Figure 3b. It can be seen that the current increases with the rise of temperature because of the thermally excited carriers, which enhance the carrier concentration in SQ NWs. The saturation current, I_0, in eq 1 can be expressed as

$$I_0 = AA^*T^2 \exp\left(-\frac{q\phi_b}{kT}\right) \quad (2)$$

where A is the Schottky contact area, A^* is the effective Richardson-constant, and Φ_b is the Schottky barrier height. It is known that the barrier height for a metal-semiconductor Schottky junction is determined by both the work function difference and the surface states. A general expression of the barrier height is given in eq 3, where the surface states are neglected:

$$\phi_b = \frac{kT}{e} \ln\left[\frac{AA^*T^2}{I_0}\right] \quad (3)$$

From eq 1, I_0 can be obtained by extrapolating the semilog $I-V$ curves at different temperatures (Figure 3c). By substituting these values into eq 3, Φ_b for the Schottky junction can be calculated, and the result is shown in Figure 3d. It is found that Φ_b increases from 0.24 to 0.79 eV as the temperature increases from 90 to 300 K. We note that this result has deviated from the conventional Schottky theory in which Φ_b should decrease with the temperature rise. Similar phenomena have been often investigated in inorganic Schottky barrier diodes, and the literally inhomogeneous barrier height was suggested as an important reason for this deviation.[48,49] The current transport across the Schottky interface is a temperature-activated process, and more carriers have sufficient energy to surmount the higher barrier with the increase of temperature. As a result, the dominant barrier height will be improved with the temperature.[50] Also, besides thermionic emission, it seems that tunneling and leakage currents need to be considered to precisely estimate the current transport in the SQ-NW array/Ti Schottky barrier. The barrier height of 0.79 eV at room temperature is a little bit smaller than the predicted value of ~1.04 eV from the band-energy diagram in Figure 2b. We speculate that the inaccuracy arising from the simple thermionic emission model described above is a possible reason. To address this issue, a more sophisticated model that considers the corrections of tunneling and leakage currents is expected to be adopted in further investigation. Meanwhile, the vacuum-level shift caused by the interfacial dipole that often been observed for organic/metal and organic/organic interfaces is likely to be another important reason responsible for this observation.[51−53]

To evaluate the performance of NW-arrays-embedded Schottky- and ohmic-type photodetectors comparatively, their light responses were investigated, as shown in Figure 4. It is noted that the conduction current increases remarkably upon white-light illumination because of the photo-induced photocurrent for both Schottky- and ohmic-type devices. However, it should be mentioned that when the Schottky-type device is reversely biased it is much more sensitive. The current of the Schottky-type device under dark conditions is about 4 orders of magnitude lower than that of the ohmic-type device at the reverse bias direction, and the current enhancement percentage upon light illumination for the Schottky-type device is also obviously larger than the corresponding ohmic-type device. The photosensitivity is defined as $(I_{light} - I_{dark})/I_{dark}$ as a percentage. As determined from Figure 4a, under white-light illumination and at a bias voltage of −5 V, the sensitivity of the Schottky-type device is found to be 12 167%, which is more than 60 times higher than that of ohmic-type device (197%). Figure 4b depicts the time-resolved photoresponse to white

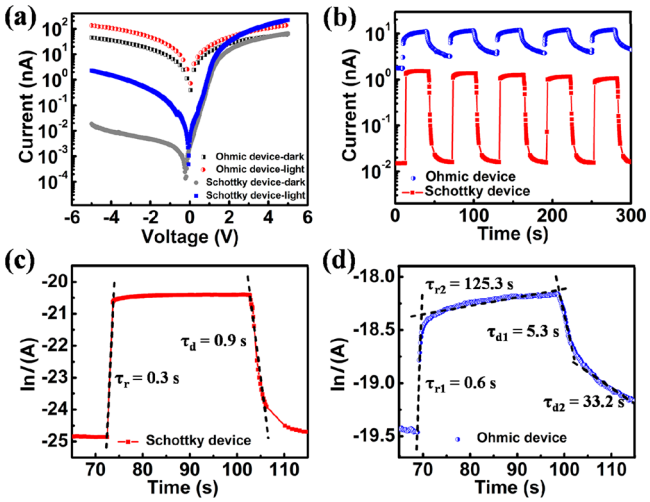

Figure 4. (a) $I-V$ characteristics of the SQ-NW-array-based ohmic- and Schottky-type devices measured in the dark and under white-light illumination (0.1 mW/cm^2), respectively. (b) Time-resolved photoresponse of the NW-array-based ohmic- and Schottky-type devices. The white-light source was turned on/off manually to generate pulsed light. (c, d) Enlarged views of the rise/decay edges of the Schottky- and ohmic-type devices, respectively.

light at a fixed bias voltage of −5 V. It reveals that the ohmic-type device shows a lower on/off ratio of approximately 3, whereas a markedly improved on/off ratio of greater than 10^2 was obtained for the Schottky-type device. This result coincides very well with the sensitivity comparison between the two devices. We note that after mutiple illumination cycles the devices still exhibit a nearly identical response, which demonstrates the high robustness and good reproducibility of the photodetectors. To determine the response time of the devices, the enlarged time-response curves are drawn in a natural logarithmic plot in Figure 4c. The linear fits to the rise and decay edges confirm the exponential time dependency following $I = I_0\ (1 - e^{-t/\tau_r})$ and $I = I_0\ e^{-t/\tau_d}$ for the photocurrent, respectively, where τ_r and τ_d are the time constants for the rise and decay edges, respectively. We note that the photocurrent rise and decay for the Schottky-type device is very steep; τ_r and τ_d were estimated to be 0.3 and 0.9 s, respectively. In contrast, the rise/decay edge of the ohmic-type device usually consists of two components(i.e., a fast-response component resulting from the rapid change of carrier concentration as soon as the light is turned on/off, and a slow-response component caused by the carrier trapping/releasing because of the existence of defects in NWs. τ_{r1}/τ_{r2} and τ_{d1}/τ_{d2} were estimated to be 0.6 s/125.3 s and 5.3 s/33.2 s, respectively, for the ohmic-type device. It was evident that the Schottky-type device provides a much faster response speed to light than that of the ohmic-type device.

From the above results, it is clear that the device structure plays an essential role in determining the device performance of the SQ-NW-array-based photodetectors. This can be understood by considering the different working mechanisms of these two types of photodetectors. In the ohmic-type device, the photogenerated electron−hole pairs are separated by the external electric field and drift toward the opposite directions, forming the photocurrent. The relatively long transit time of the carriers as well as the existence of carrier-trapping centers are responsible for the lower switching speed of this type of device. Also, its photosensitivity is relatively low because of the

large dark current. In contrast, for the Schottky-type device the photogenerated carriers are separated at the junction interface by the strong built-in electric field; holes drift into the NWs, whereas electrons inject into the Ti electrode. It is evident that the presence of a strong built-in electric field at the junction interface can greatly facilitate the carrier separation/transport, giving rise to a fast switching speed. Because of the ultralow dark current at the revised bias direction for a Schottky diode, the sensitivity of the Schottky-type device is remarkably improved as compared to the ohmic-type device. Therefore, Schottky-type devices can possess large response sensitivity and high switching speed, which are both key issues for their modern device applications in the fields of optical communication, imaging, and so on.

To explore further the potential merits of the SQ-NW-array/Ti Schottky-type photodetectors, we also fabricated single SQ-NW-based Schottky diodes for light sensors, which were fabricated using the same method as that for the NW-array-based devices except for the lower solution concentration and much slower evaporation rate during the NW growth. The inset in Figure 5a shows a typical optical microscope image of the

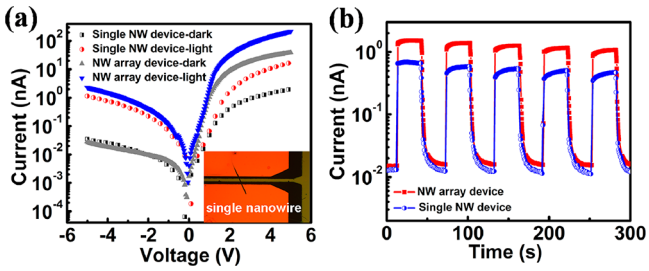

Figure 5. (a) $I-V$ characteristics of the Schottky-type devices fabricated from both a SQ-NW array and a single NW. Measurements were conducted in the dark and under white-light illumination (0.1 mW/cm^2), respectively. The inset shows the optical microscope image of the single NW-based Schottky-type device. (b) Time responses of the Schottky-type devices based on a NW array and a single NW, respectively. The voltage bias was fixed at −5 V during the measurements.

device. Interestingly, the sensitivity of the NW-array-based Schottky-type device (12 167%) was almost 4 times higher than that of the single NW-based device counterpart (3194%) under the same conditions as determined from Figure 5a. The photocurrent in the NW-array-based device is remarkably enhanced because of the higher light-absorption area, verifying the superiority of the array-based Schottky-type device for light sensors. However, from Figure 5b, the response speed of the NW-array-based device is almost identical to the single NW-based device. This result shows that although more defects and impurities might be introduced into the NW-array-based device the unique in situ device-integration technique still guarantees the high quality of the Schottky junction. Moreover, because each NW can form an individual Schottky diode in the NW array, the parallel connection of these single NW diodes will largely suppress the performance fluctuation of the NW-array-based devices by taking advantage of the average effect, giving rise to the high stability and reproducibility of the device.

To characterize further the SQ-NW-array-based Schottky-type photodetectors, the light-intensity-dependent photocurrent was measured. Figure 6a shows the $I-V$ curves measured under different light intensities at an excitation wavelength of 600 nm. It can be seen that the device shows

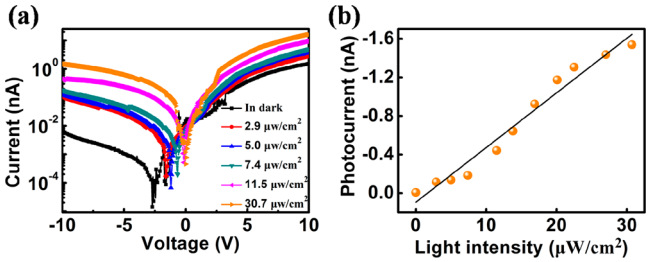

Figure 6. (a) $I-V$ characteristics of a SQ-NW-array-based Schottky-type device measured at varied light intensities from 0 to 30.7 μw/cm^2. The light wavelength is 600 nm. (b) Plot of the photocurrent as a function of the light intensity under an excitation wavelength of 600 nm and a fixed bias voltage of −5 V.

good light-controlled characteristics and the photocurrent increases with the increase in the light intensity, revealing an approximately linear relation. Significantly, owing to the high device sensitivity, the Schottky-type device exhibits excellent low-light detection properties and is capable of detecting light with a density as low as 2.9 μW/cm^2. This characteristic is important and shows the potential for developing low-light photodetectors based on organic nanostructures in the future.

The assembly of NWs with a reasonable alignment, density, and uniformity is always one of the major challenges toward NW-based large-scale electronics and optoelectronics. By implementing the evaporation-induced patterning technology for the periodical growth of NW arrays on prefabricated electrodes, large-area NW arrays can be assembled at well-defined locations, forming Schottky-type devices on the substrate, and they can be configured as an integrated photodetector circuitry. Figure 7a shows the optical microscope image of the integrated devices, where it can be seen that the eyelash-like SQ-NW arrays can span across the electrode pairs perfectly. The photodetector circuitry was measured at both the single-device component and circuit level to characterize their operational performance. It is noted that although the devices are connected in parallel by the SQ-NW array the distance of the adjacent devices in the parallel direction (250 μm) is much larger than the interspaces of the Au−Ti electrode pairs (15 μm for rows 1 and 3 and 60 μm for row 2). Taking into consideration the low conductivity of the organic SQ NWs, the leakage current between adjacent devices should be very low and would not affect the test result at each pixel. By applying the voltage between −5 V and +5 V, the rectification ratio of the Schottky-type device at each pixel was measured in the dark, and the distribution is shown in Figure 7b. Notably, the circuitry demonstrates a high uniformity with a mean rectification ratio of around 1200−1500. The distribution of pixel photosensitivity in Figure 7c also shows that most of the functional devices have almost the same sensitivity with a very small pixel-to-pixel variation that arises from the high uniformity of the assembled NW arrays. The high yield of the operational pixels with a high level of integration unambiguously demonstrates the potential of this assembly strategy for large-scale sensor and optoelectronic device integration.

CONCLUSIONS

Using an evaporation-induced self-assembly method, large-scale SQ-NW arrays could be selectively grown on prefabricated electrodes with controlled interspacing, and they can be configured as integrated photodetector circuitry. Through

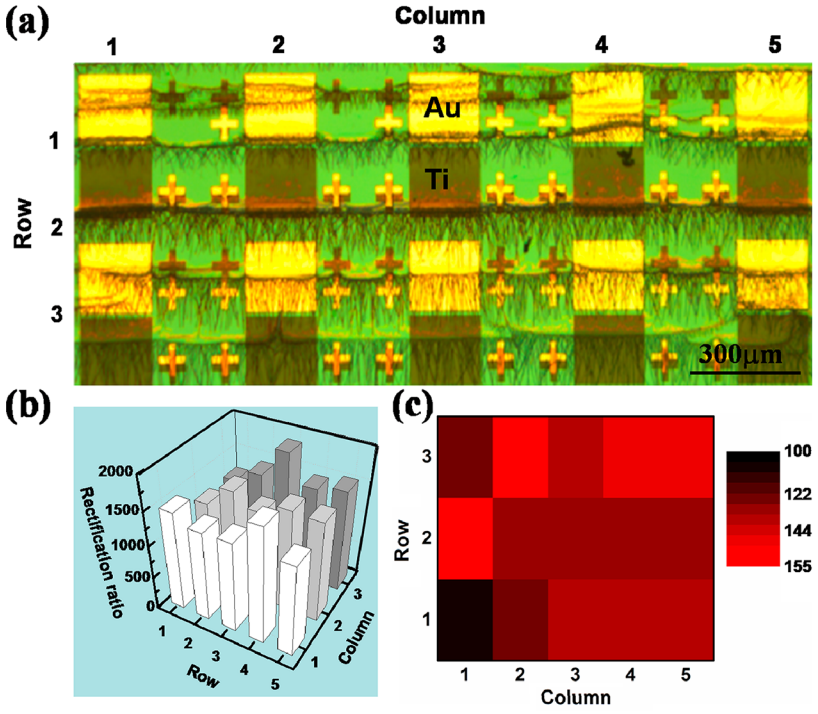

Figure 7. (a) Optical microscope image of the integrated Schottky-type devices fabricated with an evaporation-induced self-assembly method. (b) Distribution of the rectification ratio for each Schottky device in the circuitry in the dark. (c) Two-dimensional contrast map showing the functional circuit elements by exposing the circuitry to an even white-light field (0.1 mW/cm^2).

electrode structure design, the SQ-NW array could form ohmic-device contacts with Au−Au electrodes and meanwhile construct Schottky-device contacts with Au−Ti electrodes. The Schottky-type device showed an excellent rectification characteristic, with a high rectification ratio of ~10^3 and a low turn-on voltage of ~0.85 V. It was found that the NW-array-based Schottky-type photodetectors exhibited a much higher sensitivity and a faster switching speed than that of ohmic-type photodetectors. The excellent performance can be attributed to the presence of the Schottky barrier at the SQ-NW array/electrode interface. More interestingly, the NW-array-based Schottky-type devices also demonstrated higher sensitivity and comparable response speed compared to single NW-based devices. This further verified their superiority for use as light sensors by taking into account the higher reliability and reproducibility of the array-based devices. The intensity-dependent photoresponse of the NW-array-based Schottky-type photodetectors were further investigated. Notably, the devices were able to detect low light with intensity as low as 2.9 μW/cm^2. These results indicate that the SQ-NW-array-based Schottky-type devices are promising candidates for applications in high-sensitivity and high-speed photodetectors and opto-electronic switches. The photodector circuits were measured at circuit level to characterize their potential applications as image sensors; very small pixel-to-pixel variation was observed in the distribution of pixel photosensitivity, which arose from the high uniformity of the assembled NW arrays. The demonstration of the in situ integration of organic NW Schottky-type photo-detectors paves the way for low-cost and high-performance organic nano-optoelectronic devices.

■ ASSOCIATED CONTENT

Ⓢ Supporting Information

SQ molecular structure and arrangement in aggregates. UPS measurements of an SQ film for estimating the HOMO and LOMO levels. This material is available free of charge via the Internet at http://pubs.acs.org.

■ AUTHOR INFORMATION

Corresponding Author

*E-mail: xjzhang@suda.edu.cn (X.J.Z.); Tel: +86-512-65880955. E-mail: xhzhang@mail.ipc.ac.cn (X.H.Z.); Tel: +86-10-82543510. E-mail: jsjie@suda.edu.cn (J.S.J.); Tel: +86-512-65881265.

Author Contributions

§These authors contributed equally. The manuscript was written through the contributions of all authors. All authors have given approval to the final version of the manuscript.

Notes

The authors declare no competing financial interest.

■ ACKNOWLEDGMENTS

This work was supported by the Major Research Plan of the National Natural Science Foundation of China (nos. 91027021 and 91233110), the National Basic Research Program of China (973 program, grant nos. 2013CB933500, 2012CB932400, 2011CB808400, and 2010CB934500), and the National Natural Science Foundation of China (nos. 51173124 and 51172151). We also thank the Natural Science Foundation of Jiangsu Province (no. BK2010003) and a project funded by the Priority Academic Program Development of Jiangsu Higher Education Institutions.

REFERENCES

(1) Sekitani, T.; Zschieschang, U.; Klauk, H.; Someya, T. *Nat. Mater.* **2010**, *9*, 1015−1022.
(2) Gorodetsky, A. A.; Chiu, C. Y.; Schiros, T.; Palma, M.; Cox, M.; Jia, Z.; Sattler, W.; Kymissis, I.; Steigerwald, M.; Nuckolls, C. *Angew. Chem., Int. Ed.* **2010**, *49*, 7090−7912.
(3) Lei, T.; Pei, J. *J. Mater. Chem.* **2012**, *22*, 785−798.
(4) Cui, Q. H.; Zhao, Y. S.; Yao, J. N. *J. Mater. Chem.* **2012**, *22*, 4136−4140.
(5) Yan, Y.; Zhao, Y. *Adv. Funct. Mater.* **2012**, *22*, 1330−1332.
(6) Zhang, C.; Zhao, Y. S.; Yao, J. N. *Phys. Chem. Chem. Phys.* **2011**, *13*, 9060−9073.
(7) Briseno, A. L.; Mannsfeld, S. C.; Ling, M. M.; Liu, S.; Tseng, R. J.; Reese, C.; Roberts, M.; Yang, Y.; Wudl, F.; Bao, Z. N. *Nature.* **2006**, *444*, 913−917.
(8) Tang, Q.; Li, H.; Liu, Y.; Hu, W. P. *J. Am. Chem. Soc.* **2006**, *128*, 14634−14639.
(9) Liu, S.; Wang, W. M.; Briseno, A. L.; Mannsfeld, S. C.; Bao, Z. N. *Adv. Mater.* **2009**, *21*, 1217−1232.
(10) Briseno, A. L.; Mannsfeld, S. C. B.; Reese, C.; Hancock, J. M.; Xiong, Y.; Jenekhe, S. A.; Bao, Z. N.; Xia, Y. N. *Nano Lett.* **2007**, *7*, 2847−2853.
(11) Jiang, L.; Hu, W. P.; Wei, Z. M.; Xu, W.; Meng, H. *Adv. Mater.* **2009**, *21*, 3649−3653.
(12) Zhou, Y.; Wang, L.; Wang, J.; Pei, J.; Cao, Y. *Adv. Mater.* **2008**, *20*, 3745−3749.
(13) Wu, S. H.; Li, W. L.; Chu, B.; Su, Z. S.; Zhang, F.; Lee, C. S. *Appl. Phys. Lett.* **2011**, *99*, 023305−023307.
(14) Luo, J.; Yan, Q.; Zhou, Y.; Li, T.; Zhu, N.; Bai, C. J.; Cao, Y.; Wang, J.; Pei, J.; Zhao, D. H. *Chem. Commun.* **2010**, *46*, 5725−5727.
(15) Zhang, X. J.; Jie, J. S.; Zhang, W.; Zhang, C.; Luo, L.; He, Z.; Zhang, X. H.; Zhang, W. J.; Lee, C. S.; Lee, S. T. *Adv. Mater.* **2008**, *20*, 2427−2432.
(16) Dong, H. L.; Zhu, H. F.; Meng, Q.; Gong, X.; Hu, W. P. *Chem. Soc. Rev.* **2012**, *41*, 1754−1808.
(17) Arnold, M. S.; Zimmerman, J. D.; Renshaw, C. K.; Xu, X.; Lunt, R. R.; Austin, C. M.; Forrest, S. R. *Nano Lett.* **2009**, *9*, 3354−3358.
(18) Wu, S. H.; Li, W. L.; Chu, B.; Su, Z. W.; Zhang, F.; Lee, C. S. *Appl. Phys. Lett.* **2011**, *99*, 023305−023308.
(19) Ramuz, M.; Tee, B. C. K.; Tok, J. B. H.; Bao, Z. N. *Adv. Mater.* **2012**, *24*, 3223−3227.
(20) Gelinck, G. H.; Huitema, H. E. A.; van Veenendaal, E.; Cantatore, E.; Schrijnemakers, L.; van der Putten, J. B.; de Leeuw, D. M. *Nat. Mater.* **2004**, *3*, 106−110.
(21) Wei, T. Y.; Huang, C. T.; Hansen, B. J.; Lin, Y. F.; Chen, L. J.; Lu, S. Y.; Wang, Z. L. *Appl. Phys. Lett.* **2010**, *96*, 013508−013510.
(22) Fan, Z. Y.; Ho, J. C.; Takahashi, T.; Yerushalmi, R.; Takei, K.; Ford, A. C.; Javey, A. *Adv. Mater.* **2009**, *21*, 3730−3743.
(23) Fang, X. S.; Bando, Y. S.; Liao, M. Y.; Zhai, T. Y. *Adv. Funct. Mater.* **2010**, *20*, 500−508.
(24) Yang, P. D.; Yan, H. Q.; Mao, S.; Russo, R.; Johnson, J.; Saykally, R.; Morris, N.; Pham, J.; He, R. R. *Adv. Funct. Mater.* **2002**, *12*, 323−331.
(25) Wang, X. D.; Summers, C. J.; Wang, Z. L. *Nano Lett.* **2004**, *4*, 423−426.
(26) Wang, C. L.; Liu, Y.; Wei, Z. M.; Li, H. X.; Xu, W.; Hu, W. P. *Appl. Phys. Lett.* **2010**, *96*, 143302−143304.
(27) Hu, Y. F.; Zhou, J.; Yeh, P. H.; Li, Z.; Wei, T. Y.; Wang, Z. L. *Adv. Mater.* **2010**, *22*, 3327−3332.
(28) Zhou, J.; Gu, Y. D.; Hu, Y. F.; Mai, W. J.; Yeh, P. H.; Bao, G.; Sood, A. K.; Polla, D. L.; Wang, Z. L. *Appl. Phys. Lett.* **2009**, *94*, 191103−191105.
(29) Chen, C. C.; Aykol, M.; Chang, C. C.; Levi, A. F. J.; Cronin, S. B. *Nano Lett.* **2011**, *11*, 1863−1867.
(30) Kim, J. D.; Yun, J. H.; Han, C. S.; Cho, Y. J.; Park, J. H.; Park, Y. C. *Appl. Phys. Lett.* **2009**, *95*, 143112−143114.
(31) Yang, B.; Guo, F. W.; Yuan, Y. B.; Xiao, Z. G.; Lu, Y. Z.; Dong, Q. F.; Huang, J. S. *Adv. Mater.* **2013**, *25*, 572−577.
(32) Fang, X. S.; Wu, L. M.; Hu, L. F. *Adv. Mater.* **2011**, *23*, 585−598.
(33) Liang, S.; Sheng, H.; Liu, Y.; Huo, Z.; Lu, Y.; Shen, H. *J. Cryst. Growth* **2001**, *225*, 110−113.
(34) Zhang, C. Y.; Zhang, X. H.; Zhang, X. J.; Fan, X.; Jie, J. S.; Chang, J. C.; Lee, C.-S.; Zhang, W. J.; Lee, S. T. *Adv. Mater.* **2008**, *20*, 1716−1720.
(35) Law, K. Y.; Bailey, F. C.; Bluett, L. J. *Can. J. Chem.* **1989**, *64*, 1607−1619.
(36) Law, K. Y. *Chem. Rev.* **1993**, *93*, 449−486.
(37) Loutfy, R. O.; Hsiao, C. K.; Kazmaier, P. M. *Photogr. Sci. Eng.* **1983**, *27*, 5−9.
(38) Ashwell, G. J.; Jefferies, G.; Hamilton, D. G.; Lynch, D. E.; Roberts, M. P. S.; Bahra, G. S.; Brown, C. R. *Nature* **1995**, *375*, 385−388.
(39) Ajayaghosh, A. *Acc. Chem. Res.* **2005**, *38*, 449−459.
(40) Ramaiah, D.; Joy, A.; Chandrasekhar, N.; Eldho, N. V.; Das, S.; George, M. V. *Photochem. Photobiol.* **1997**, *65*, 783−790.
(41) Bigelow, R. W.; Freund, H. J. *Chem. Phys.* **1986**, *107*, 159−174.
(42) Steudel, S.; Myny, K.; Arkhipov, V.; Deibel, C.; De Vusser, S.; Genoe, J.; Heremans, P. *Nat. Mater.* **2005**, *4*, 597−600.
(43) Stallinga, P.; Gomes, H. L.; Murgia, M.; Müllen, K. *Org. Electron.* **2002**, *3*, 43−51.
(44) Drechsel, J.; Pfeiffer, M.; Zhou, X.; Nollau, A.; Leo, K. *Synth. Met.* **2002**, *127*, 201−205.
(45) Takshi, A.; Dimopoulos, A.; Madden, J. D. *Appl. Phys. Lett.* **2007**, *91*, 083513−083515.
(46) Ma, R. M.; Dai, L.; Huo, H. B.; Xu, W. J.; Qin, G. G. *Nano Lett.* **2007**, *7*, 3300−3304.
(47) Smit, G. D. J.; Rogge, S.; Klapwijk, T. M. *Appl. Phys. Lett.* **2002**, *81*, 3852−3854.
(48) Sharma, R. *J. Electron Dev.* **2010**, *8*, 286−292.
(49) Yildirim, N.; Korkut, H.; Türüt, A. *Eur. Phys. J.: Appl. Phys.* **2009**, *45*, 10302−10308.
(50) Wang, L.; Lu, M.; Wang, X. A.; Yu, Y. Q.; Zhao, X. Z.; Lv, P.; Song, H. W.; Zhang, X. W.; Luo, L. B.; Wu, C. Y.; Zhang, Y.; Jie, J. S. *J. Mater. Chem. A.* **2013**, *1*, 1148−1154.
(51) Ishii, H.; Sugiyama, K.; Ito, E.; Seki, K. *Adv. Mater.* **1999**, *11*, 605−625.
(52) Kaji, T.; Takenobu, T.; Morpurgo, A. F.; Iwasa, Y. *Adv. Mater.* **2009**, *21*, 3689−3693.
(53) Pfeiffer, M.; Leo, K.; Zhou, X.; Huang, J. S.; Hofmann, M.; Werner, A.; Blochwitz-Nimoth, J. B. *Org. Electron.* **2003**, *4*, 89−103.